Soft Matter

ROYAL SOCIETY OF CHEMISTRY

PAPER

View Article Online
View Journal

Cite this: DOI: 10.1039/d6sm00031b

Enhancing electromechanical responsiveness of PVC gels *via* ion size control

Kazuki Takahashi, Osamu Urakawa * and Tadashi Inoue

Soft electroactive polymer materials are of great interest for soft robotics and biomedical applications because of their large deformability and fast response. Plasticized poly(vinyl chloride) (PVC) gels, particularly PVC/dibutyl adipate (PVC/DBA) gels, exhibit significant bending deformation under relatively low electric fields. In this study, we enhanced the electromechanical response of PVC/DBA gels by adding salts with controlled ion sizes, including ionic liquids and lithium salts. Rheological measurements revealed a critical gelation concentration (PVC weight fraction) of w = 0.013 and a fractal dimension of 1.88. At a fixed PVC concentration (w = 0.143) corresponding to a post-gel state, salt addition (5.4×10^{-6} mol g^{-1}) increased electrical conductivity by approximately fivefold without significantly affecting elasticity. All gels showed anode-directed bending under an DC electric field, with deformation magnitudes more than five times larger than those of salt-free gels. The most pronounced bending was observed for gels containing a small anion, bis(fluor sulfonyl)imide, and a large cation, 1-ethyl-3-methylimidazolium, which is attributed to asymmetric effective charge densities formed in the electric double layer at the electrodes. These results demonstrate that the ion size control of added salts is an effective strategy for enhancing the electromechanical performance of PVC/DBA gels under low electric fields.

Received 13th January 2026,
Accepted 2nd June 2026

DOI: 10.1039/d6sm00031b

rsc.li/soft-matter-journal

1. Introduction

Smart soft materials have emerged as a rapidly growing class of functional systems that can undergo controlled changes in shape, mechanical properties, or transport behavior under external stimuli. These materials are increasingly studied in soft robotics, flexible electronics, biomedical devices, and artificial organs, owing to their adaptability and biocompatibility.[1–13] Among various stimuli, electric-field responsive gels are particularly intriguing because electrical signals can be applied with high spatial and temporal precision, enabling fast and reversible actuation.

Over the past few decades, diverse polymer gel systems have been developed to achieve electro-mechanical coupling. Polyelectrolyte gels, such as poly(acrylamide-*co*-sodium acrylate), exhibit bending in response to electric fields due to ion migration and osmotic pressure gradients.[14] Ionic polymer–metal composites (IPMCs), based on perfluorinated ionomers like Nafion, display significant bending at relatively low voltages, driven by hydrated cation migration.[15–17] Conducting polymer gels, such as polypyrrole and polyaniline, deform through electrochemical redox reactions coupled with ion insertion/extraction.[18,19]

Another important development is the ''Bucky gel actuator,'' which consists of electrodes made from single-walled carbon nanotubes (SWCNTs) mixed with ionic liquids to form a conductive gel, combined with a polymer electrolyte layer.[20–22] In these actuators, an applied electric field drives ion migration within the ionic liquid, leading to asymmetric swelling of the CNT–gel electrodes and producing efficient bending motion. Bucky gel actuators are notable for their low-voltage operation (<3 V), large strain, and high durability, making them strong candidates for artificial muscles and micro-robotics.

Within this broader context, poly(vinyl chloride)/dibutyl adipate (PVC/DBA) gels represent a distinctive class of electro-responsive gels. Unlike polyelectrolytes, IPMCs, or conducting polymer systems, PVC/DBA gels are neutral polymer/plasticizer systems, yet they exhibit pronounced creeping, electro-wetting, and bending deformation under electric fields.[23–26] Their low density, flexibility, and processability make them attractive for applications such as artificial muscles, tunable lenses, and artificial pupils. Previous work by Hirai and colleagues suggested that the deformation of PVC/DBA gels is linked to the migration of negatively charged species associated with the plasticizer.[23,27–29] Although DBA migration was observed under electric fields, the chemical identity of the mobile carriers has not been conclusively established. This uncertainty regarding

Department of Macromolecular Science, Graduate School of Science, The University of Osaka, 1-1 Machikaneyama-cho, Toyonaka, Osaka 560-0043, Japan.
E-mail: urakawa@chem.sci.osaka-u.ac.jp

the origin of the charges represents a key challenge in understanding the electro-responsive mechanism of PVC/plasticizer gels.

Subsequent studies proposed that ion size asymmetry could be a critical factor. Zheng *et al.* suggested that large anions broaden the ion layer at the anode, enhancing wettability, while smaller cations produce denser ion layers at the cathode, reducing contact area, thereby driving deformation.[30] However, their theoretical framework relies on simplified interfacial assumptions and dilute-ion conditions that may not fully capture the complex ion–polymer and ion–plasticizer interactions inherent to highly plasticized PVC systems. Consequently, the predicted ion-size dependence of interfacial charge accumulation has not yet been experimentally verified and remains open to further examination. Electroacoustic measurements further supported asymmetric ion accumulation, but without chemical identification of the species involved.[23,29]

A practical limitation of PVC/DBA gels is their requirement for high operating voltages (several tens of V mm^{-1}). To overcome this, researchers have introduced ionic liquids,[31] carbon nanotubes,[32] and other conductive additives[33,34] to reduce the voltage threshold. While these composites improve actuation efficiency, they introduce heterogeneity and phase separation, making it difficult to derive a unified mechanistic understanding. Compared to polyelectrolytes, IPMCs, and conducting polymers—where the roles of mobile ions and redox processes are relatively well understood—the origin of electro-response in PVC/plasticizer gels remains elusive.

In the present study, we systematically introduced ionic liquids or solid salts that dissolve homogeneously into PVC/DBA gels, thereby minimizing the contribution of unknown pre-existing ions. By selecting salts with controlled cation and anion sizes, we investigated how ion size and mobility influence interfacial charge accumulation and electro-deformation. Our objectives are twofold: (i) to identify the dominant charge carriers and clarify the underlying mechanism of electro-response in PVC gels, and (ii) to establish design guidelines for achieving low-voltage actuation in homogeneous gel systems.

More importantly, the present study addresses a fundamental unresolved question in PVC/plasticizer gel actuators: whether the electromechanical deformation is governed simply by the total amount of accumulated interfacial charge, or by ion-size-dependent asymmetric charge distributions formed near the electrodes under high electric fields. In addition, previous studies on PVC/plasticizer gels have suggested that redistribution of the plasticizer component may also contribute to the deformation behavior. By systematically varying both cation and anion sizes in homogeneous PVC/DBA/salt gels, we clarify how ion size influences electrical double layer formation, charge asymmetry, and bending deformation, while discussing their possible coupling with plasticizer redistribution. Through this approach, the present work establishes a mechanistic framework for understanding electro-responsive deformation in neutral polymer/plasticizer gels, in addition to improving actuation performance.

2. Experimental

2.1. Materials

Polyvinyl chloride (PVC) (M_w ~233 000, M_n ~99 000, Sigma-Aldrich, Co., USA) was used as the polymer matrix. Dibutyl adipate (DBA) (Tokyo Chemical Industry Co., Ltd. Japan) served as the plasticizer. Tetrahydrofuran (THF) (Fujifilm Wako Pure Chemical Corp. Japan) was employed as the solvent for gel preparation. To control the ionic species in the gel, four different salts (shown in Fig. 1) were incorporated: 1-ethyl-3-methylimidazolium bis(trifluoromethanesulfonyl)imide (EMIM-TFSI; Kanto Chemical Co., Inc., Japan), lithium bis(trifluoromethanesulfonyl)imide (Li-TFSI; Fujifilm Wako Pure Chemical Corp., Japan), 1-ethyl-3-methylimidazolium bis(fluorosulfonyl)imide (EMIM-FSI; Fujifilm Wako Pure Chemical Corp., Japan), and lithium bis(fluorosulfonyl)imide (Li-FSI; Fujifilm Wako Pure Chemical Corp., Japan). All chemicals were used as received, without further purification.

2.2. Preparation of Gel Samples

PVC/DBA gels were prepared with PVC : DBA weight ratios ranging from 9 : 1 to 1 : 75, corresponding to PVC weight fraction (w_{PVC}) from 0.900 to 0.0132. A specified amount of PVC and DBA was dissolved in tetrahydrofuran (THF) at a weight ratio of approximately 4 to 20 times the total weight of the polymers. The mixture was stirred for 2–3 days until visually homogeneous solutions without observable precipitation or phase separation were obtained. The resulting solution was cast into a square Teflon dish (8 × 8 × 1 cm^2) and left to stand in air at room temperature for 3–5 days. Residual solvent was then removed by vacuum drying at room temperature for 1 day, yielding square PVC/DBA gel films with a thickness of approximately 2 mm.

For the PVC/DBA/salt gels, the PVC : DBA ratio was fixed at 1 : 6 (w_{PVC} = 0.143). Salts were incorporated at weight fractions (w_{salt}) of 0.01–0.1 relative to the combined mass of PVC and DBA. The preparation procedure was the same as that described above: the THF solution was cast and dried to obtain gel films. All resulting gel films were visually confirmed to be transparent and homogeneous, with no observable phase

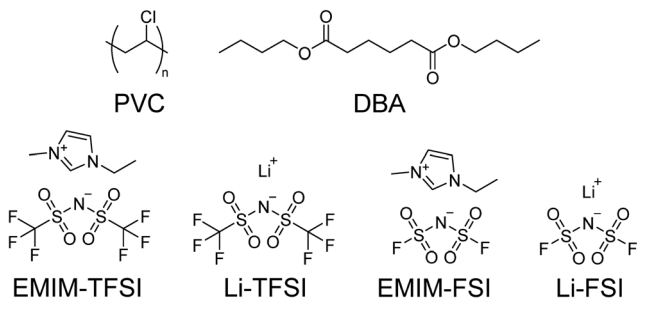

Fig. 1 Chemical structures of samples used in this study: poly(vinyl chloride) (PVC), di-*n*-butyl adipate (DBA), 1-ethyl-3-methylimidazolium bis(trifluoromethanesulfonyl)imide (EMIM-TFSI), lithium bis(trifluoromethanesulfonyl)imide (Li-TFSI), 1-ethyl-3-methylimidazolium bis(fluorosulfonyl)imide (EMIM-FSI), and lithium bis(fluorosulfonyl)imide (Li-FSI).

separation or salt precipitation. In these ternary systems, w_{PVC} varied slightly depending on the amount of added salt. To enable comparison of electrical characteristics among different salts, additional gels were prepared at a constant salt molar concentration (n_{salt} = 5.35 × 10^{-6} mol g^{-1}), which corresponds to w_{salt} = 0.0010 for Li-FSI. Here, n_{salt} is defined as the molar amount of salt per gram of the total gel sample.

2.3. Viscoelastic measurement

Rheological measurements were conducted to determine the elastic modulus of the prepared gels. The storage and loss moduli (G' and G'') were measured over an angular frequency range of 1.00 × 10^{-1} s^{-1} ~ 1.00 × 10^{2} s^{-1} using a stress-controlled rheometer (MCR302, Anton Paar, Austria) equipped with a 25 mm diameter parallel plate fixture. The applied strain amplitude (γ) was varied between 0.5% and 10%.

For PVC/DBA gels, measurements were conducted for samples with w_{PVC} ranging from 0.013 to 0.16. For the PVC/DBA/salt gels, four different salts were incorporated into PVC : DBA = 1 : 6 gels, with w_{salt} adjusted from 0.0010 to 0.10, and these samples were subjected to rheological characterization.

2.4. Dielectric measurement

Dielectric relaxation measurements were performed to investigate the electrical properties of the gels. The complex permittivity was measured using a dielectric analyzer (Alpha-A, Novocontrol Technologies GmbH & Co. KG, Germany) with an applied AC voltage ranging from 0.001 to 3 V and a frequency range of 1.0 × 10^{-3} to 2.6 × 10^{6} Hz. The thickness of the gel films used for these measurements was 1.2–1.7 mm.

Nonlinear dielectric properties under high voltage were examined using the current absorption method. A square-wave voltage of 170 V was applied, and the complex permittivity was determined for the PVC/DBA gel (PVC : DBA = 1 : 6) and for all PVC/DBA/salt gels (PVC : DBA = 1 : 6, n_{salt} = 5.35 × 10^{-6} mol g^{-1}) at frequencies ranging from 1.6 × 10^{-4} to 1.4 × 10^{-2} Hz (ω = 0.001–0.086 s^{-1}). The gel thickness was 1.25–1.35 mm. Samples were placed between gold-plated stainless-steel electrodes with a diameter of 18 mm, and the transient current, $i'(t)$, passing through the sample was recorded. The electrode cell and representative time-dependent current data are shown in Fig. S3. The net current was obtained as $i(t) = i'(t) - i_\infty$, where i_∞ denotes the leakage current. The after-effect function $\phi(t)$ was then calculated as

$$\phi(t) = \frac{i(t)}{C_0 V} \quad (1)$$

where C_0 is the geometric capacitance of the dielectric capacitor and V is the applied DC voltage. The real and imaginary parts of the permittivity were subsequently obtained from $\phi(t)$ according to

$$\varepsilon'(\omega) - \varepsilon_s = \int_0^\infty \phi(t) \cos \omega t \mathrm{d}t \quad (2)$$

$$\varepsilon''(\omega) = \int_0^\infty \phi(t) \sin \omega t \mathrm{d}t \quad (3)$$

where ε_s is the high-frequency dielectric constant. The time resolution of the voltmeter was 0.05 s, and the calculations were performed using dt = 0.05 s.

2.5. Evaluation of electric field response

The electro-mechanical response of PVC/DBA gels and PVC/DBA/salt gels (PVC : DBA = 1 : 6, n = 5.35 × 10^{-6} mol g^{-1}) was evaluated using a stainless-steel electrode with one rounded end (radius of curvature: 1.5 mm), as shown in Fig. 2. A silicon rubber spacer was placed between the electrodes to maintain a 1 mm inter-electrode gap. Gel samples were cut into strips (15 mm × 2 mm, thickness: 1.2–1.4 mm) and mounted between the electrodes, leaving ~5 mm of the strip protruding (Fig. 2). To track the deformation process of the gel using image analysis software (ImageJ), the free end of each gel strip was stained with graphite and monitored using a CCD camera (Nikon Digital Sight 1000, resolution: 0.04 s).

An electric field was applied using a function generator (WAVE FACTORY WF 1944, NF Corporation, Japan) connected to a high-speed high-voltage amplifier (HVA4321, NF Corporation, Japan). The applied field and the current passing through the sample were recorded at 0.05 s intervals using a data logger (midi LOGGER GL260, Graphtec Corporation, Japan).

Square-wave voltages were applied, and an experiment was conducted where a constant voltage was applied at t = 0. Under sufficient field strength, all gels exhibited bending toward the

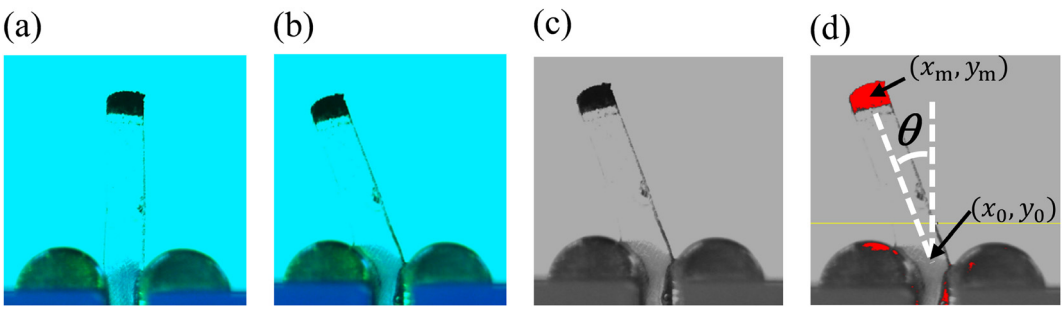

Fig. 2 (a) Photograph of a gel strip placed between the stainless electrodes by a 1 mm gap before bending. (b) Bending of the gel toward the anode under an applied electric field. (c) Grayscale scale converted image of the gel shown in (b). (d) Detection of the graphite-stained gel tip by thresholding the grayscale image in (c); the red area indicates the detected area used for determining the bending angle θ.

anode (Fig. 2b). Snapshots from the recorded videos were analyzed with ImageJ. The bending angle (θ) was calculated from the center of mass coordinates of the graphite-stained tip (x_m,y_m) relative to the reference point at the gel base (x_0,y_0), defined as the midpoint of the line connecting the electrode tips, according to eqn (4).

$$\theta = \tan^{-1}\left(\frac{x_m - x_0}{y_m - y_0}\right) \quad (4)$$

3. Results and discussion

3.1. Concentration dependence of elastic modulus

The frequency dependence of the storage modulus (G') and loss modulus (G'') for PVC/DBA gels (PVC : DBA = 1 : 1 to 1 : 75, corresponding to PVC weight fractions w_{PVC} = 0.013–0.5) is shown in Fig. 3(a) and (b), respectively. For w_{PVC} = 0.013, the data exhibit behavior characteristic of a critical gel, which can be described by a power-law relation as reported by Martin *et al.*:[35]

$$G'(\omega) \sim G''(\omega) \sim \omega^n \quad (5)$$

Furthermore, according to the Kramers–Kronig relation,

$$\tan\delta = \frac{G''}{G'} = \tan\left(\frac{n\pi}{2}\right) \quad (6)$$

At the gelation point, $\tan\delta$ becomes independent of ω. Thus, when $\tan\delta$ is plotted at various frequencies across a concentration range near the gelation point, all curves should intersect at a single point. This is demonstrated in Fig. 4. From this analysis, the critical gelation point was determined as $w_{PVC,G}$ = 0.0152. From the observed value of $\tan\delta$ = 1.62, the power-law exponent n is calculated as n = 0.647. The dashed line in Fig. 3 indicates this slope, showing good agreement with the data for w_{PVC} = 0.013. According to Muthukumar's theory,[36] when excluded volume effects and hydrodynamic interactions are screened, the relationship between n and the fractal dimension d_f in d-dimensional space is given by:

$$n = d(d + 2 - 2d_f)/2(d + 2 - d_f) \quad (7)$$

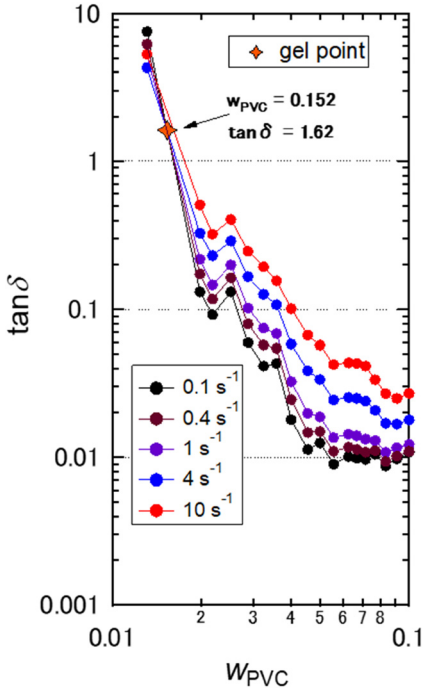

Fig. 4 The dependence of $\tan\delta$ on the PVC weight fraction (w_{PVC}) at different angular frequencies.

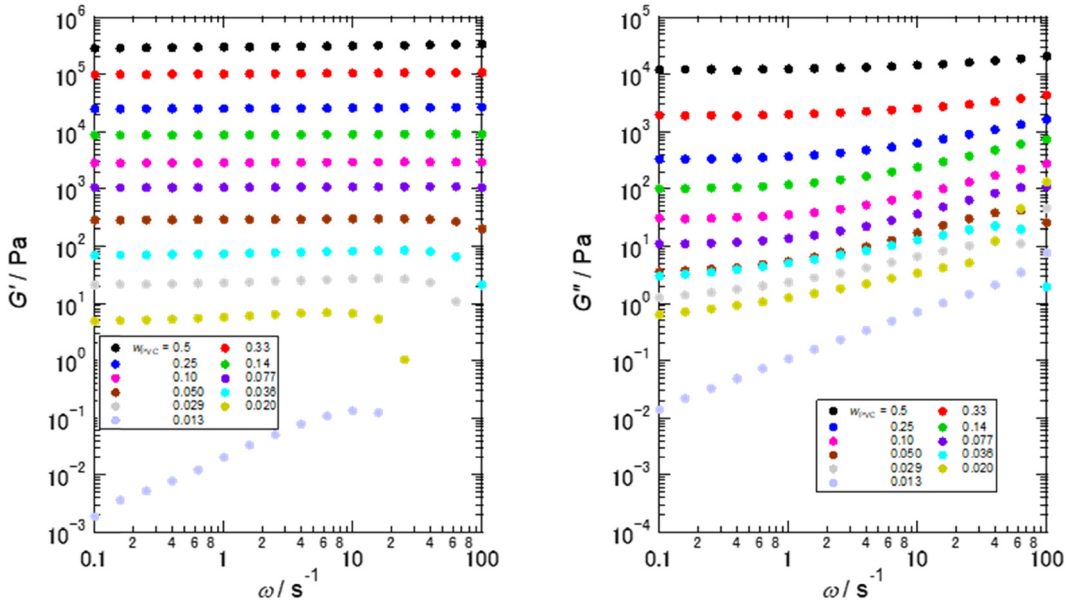

Fig. 3 Storage and loss moduli (G' and G'') of PVC/DBA gels with the PVC fraction, w_{PVC} = 0.013–0.500.

Substituting $n = 0.647$ and $d = 3$, the fractal dimension was obtained as $d_f = 1.81$. This value is smaller than 2 (the value for a Gaussian chain), it suggests that the PVC/DBA gel possesses a slightly expanded, fractal-like network structure. These results demonstrate that the PVC/DBA system undergoes a well-defined gelation transition and forms a fractal-like network structure near the critical gel point.

Fig. 5(a) shows the dependence of the plateau modulus (G_N) on w_{PVC} for concentrations $w_{PVC} \geq 0.0196$. In this double-logarithmic plot, the relation between G_N and w_{PVC} is not linear but exhibits a downward concavity. Therefore, Fig. 5(b) presents G_N as a function of the relative distance from the gelation point (ϵ) defined as:

$$\epsilon = \frac{w_{PVC} - w_{PVC,G}}{w_{PVC,G}} \quad (8)$$

This plot shows that the data can be fitted with a straight line that satisfies the power-law relationship $G_N \sim \epsilon^{2.66}$. If we denote this exponent of the elastic modulus as t, it is related by Colby & Rubinstein's scaling theory:[37]

$$t = \nu d \quad (9)$$

here, ν is the critical exponent of the correlation length ξ ($\xi \sim \epsilon^{-\nu}$), and it is known that $\nu \approx 0.88$ for a three-dimensional system. Thus, $t = 2.64$, which is consistent with the experimental value. The observed scaling behavior indicates that the elasticity development of the PVC/DBA gels follows critical gelation behavior consistent with percolation-based scaling theory.

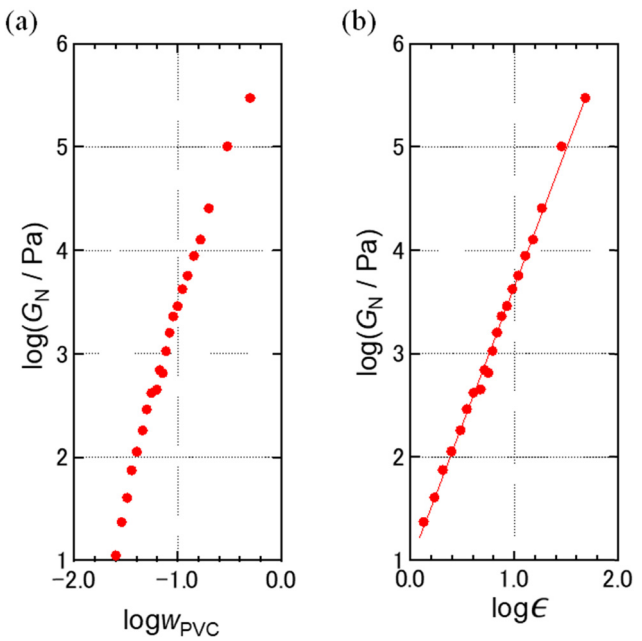

Fig. 5 (a) Dependence of the plateau storage modulus, G_N, on the PVC weight fraction, w_{PVC}. (b) Dependence of the plateau storage modulus, G_N, on the relative distance from the gelation point, ϵ.

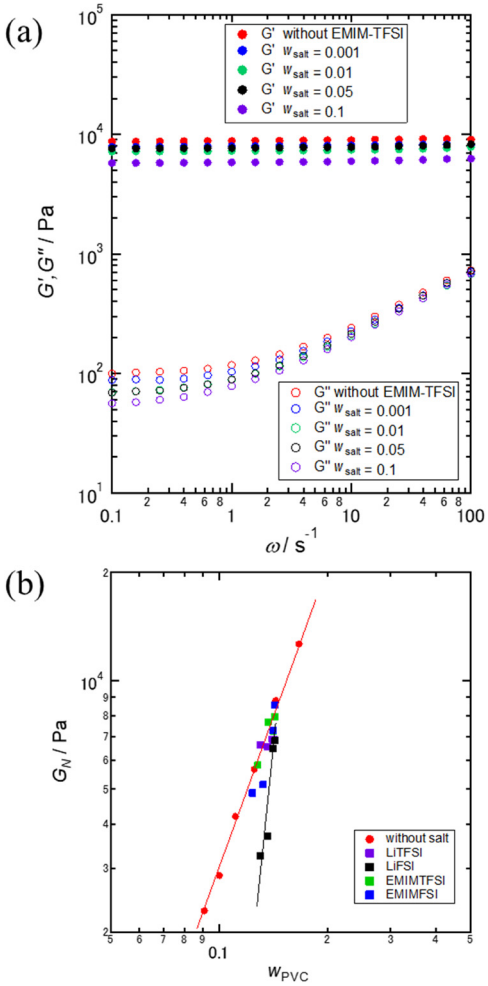

Fig. 6 (a) Frequency dependence of G' (filled circles) and G'' (open circles) for PVC/DBA/EMIM-TFSI gels with salt concentrations of w_{salt} = 0.0010–0.100 at a fixed PVC : DBA ratio of 1 : 6. (b) Dependence of the plateau modulus, G_N, on w_{PVC} for the PVC/DBA/salt systems (PVC : DBA = 1 : 6, w_{salt} = 0–0.100). In the salt-containing systems, w_{PVC} changes with increasing salt concentration because the PVC : DBA ratio was fixed at 1 : 6. Red circles represent data for the PVC/DBA gels, in which w_{PVC} was varied by changing the PVC : DBA ratio.

As a representative example of the salt-containing systems, the viscoelastic spectra of PVC/DBA/EMIM-FSI gels are shown in Fig. 6(a). Similar to PVC/DBA gels, G'remained constant across the angular frequency range of 1.00×10^{-1} s^{-1}–1.00×10^{2} s^{-1} for all concentrations. A systematic decrease in G' was observed with increasing salt concentration. This decrease can mainly be attributed to the fixed PVC : DBA ratio of 1 : 6; as salt was added, the effective PVC concentration decreased accordingly.

Fig. 6(b) presents the dependence of the plateau modulus G_N on w_{PVC}. All salt-containing systems except for PVC/DBA/Li-FSI showed comparable reduction in G_N, which can be largely attributed to the decrease in the effective PVC concentration resulting from salt addition. In contrast, the PVC/DBA/Li-FSI system exhibited the most pronounced decrease. This behavior may be related to the small ionic radius and high charge

Table 1 The values of w_{salt}, G_N, and σ_N, where σ_N is the plateau conductivity, in the system with PVC/DBA gel (PVC : DBA = 1 : 6 corresponding to w_{PVC} = 0.143) and PVC/DBA/salt gels (n_{salt} = 5.35 × 10^{-6} mol g^{-1})

Salt	Without salt	Li-TFSI	EMIM-TFSI	Li-FSI	EMIM-FSI
w_{salt}	0	0.00153	0.00209	0.000999	0.00153
G_N/kPa	8.91	6.98	8.01	6.94	8.66
10^7 σ_N/S cm^{-1}	1.45	7.24	9.48	9.31	10.6

density of both the Li^+ ions and FSI^- ions, which are likely to interact with PVC chains, inhibit the formation of PVC microcrystals, and consequently lower the crosslinking density, resulting in reduced G' values.

At the lowest salt concentration, as shown in Table 1, the influence of salt addition on G' was negligible for all salts investigated. These concentrations were adjusted to give a constant molar concentration of n_{salt} = 5.35 × 10^{-6} mol g^{-1}. This specific concentration was selected for subsequent electric-field-induced gel deformation experiments because the elastic modulus remained largely unaffected by salt addition. Furthermore, the PVC : DBA = 1 : 6 composition corresponds to the composition exhibiting the highest dielectric constant and conductivity, as will be in the following section. These results indicate that the selected experimental conditions minimize differences in elastic modulus among the samples, allowing the subsequent electromechanical behavior to be discussed primarily in terms of ionic and interfacial effects rather than viscoelastic stiffness differences.

3.2 Dielectric relaxation behavior

Fig. 7(a) and (b) show the frequency dependence of the dielectric constant (ε') and conductivity (σ') for PVC/DBA gels with w_{PVC} ranging from 0 to 0.9. The pronounced rise in ε' at low frequencies, together with the nearly frequency-independent σ' in the intermediate range—followed by a slight decrease at lower frequencies—is attributed to electrode polarization caused by mobile charges within the gel, rather than to dipole orientation polarization, as evidenced by the extraordinarily large ε' values at low frequencies on the order of 10^4–10^6.

As the PVC concentration increases from neat DBA, the low frequency ε' value increases, and the onset frequency of the ε' rise shifts to higher frequencies. Both ε' and the rise frequency reach a maximum at PVC : DBA = 1 : 6 (w_{PVC}), after which they decrease with further increase in PVC content. Similarly, the low-frequency plateau value of σ' (which corresponds to the DC conductivity, σ_N) also attains its maximum at w_{PVC} = 0.144.

Fig. 8(a) and (b) summarize the dependence of ε' and σ_N on w_{PVC} at 0.1 Hz, respectively. Both parameters clearly peak at the PVC : DBA = 1 : 6 composition. This concentration dependence can be rationalized by the competition between an increase in the number of charge carriers provided by the PVC component and a reduction in carrier mobility due to the higher viscosity at larger PVC fractions.

Considering that the PVC/DBA = 1 : 6 gel exhibits high conductivity and a storage modulus on the order of 10^4 Pa—providing sufficient mechanical integrity for handling—this composition was selected for subsequent electric field-induced deformation experiments. In the following, we designate the charge carriers intrinsic to PVC as "intrinsic carriers" and those introduced by added salts as "salt carriers".

Fig. 9 presents dielectric spectra of PVC/DBA/salt gels containing four different salts with n_{salt} = 5.35 × 10^{-6} mol g^{-1}. The addition of salt shifts the electrode polarization relaxation toward higher frequencies, whereas the low-frequency dielectric constant ε' shows little variation with salt addition. The dependence on salt concentration is illustrated in Fig. S1 for the PVC/DBA/EMIM-TFSI systems. As the salt concentration increases, the relaxation frequency shifts to higher frequencies, however, ε' remains nearly independent of concentration. According to Macdonald's theory of electrode polarization, ε' is expected to increase proportionally with salt concentration.[38–40] Our results deviate from this prediction, most likely because the condition of sufficiently low salt concentration—an assumption of Macdonald's model—is not satisfied in this system. This implies that the charge density of the effective electrical double layer at the electrode interface approaches saturation, regardless of the presence or absence of added salt.

Regarding the σ' data (Fig. 9c), the plateau values corresponding to σ_N for salt added gels are 4–6 times higher than that

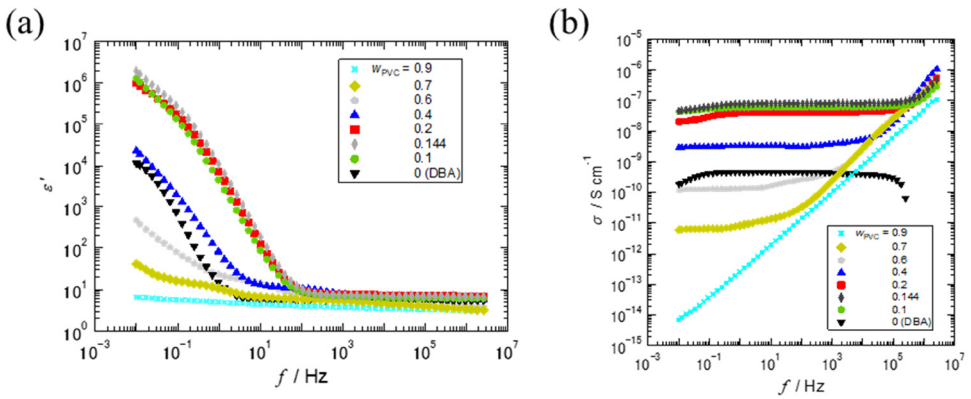

Fig. 7 Frequency dependence of (a) the dielectric constant, ε', and (b) the conductivity, σ', for PVC/DBA gels (w_{PVC} = 0–0.90).

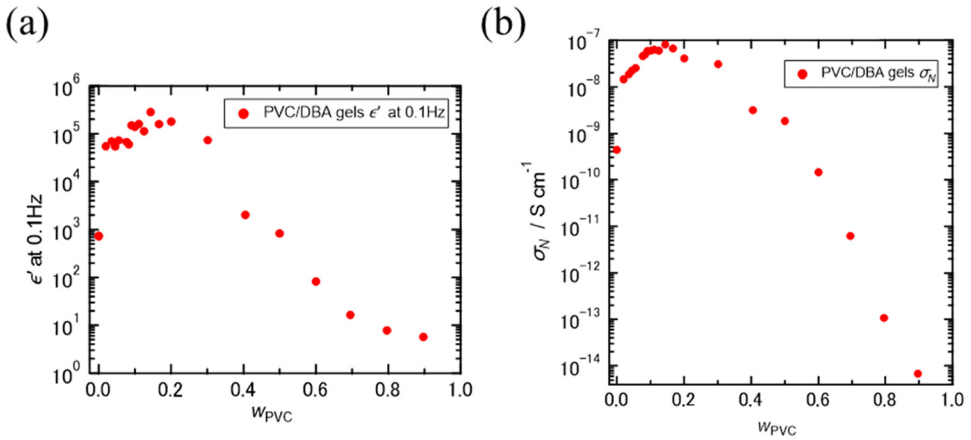

Fig. 8 w_{PVC} dependence of (a) the dielectric constant, ε', measured at 0.1 Hz and (b) the conductivity, σ_N, for PVC/DBA gels.

of the salt-free system as summarized in Table 1. These results clearly indicate that the added salt serves as the dominant factor in determining electrical conductivity and, consequently, the electrode polarization. These findings suggest that the added salts dominate charge transport and electrode polarization behavior in the PVC/DBA gels, providing the basis for the ion-species-dependent electromechanical response discussed in the following sections.

Fig. 10a shows the double logarithmic plot of σ_N for PVC/DBA/salt gels as a function of n_{salt}. It is evident that σ_N depends solely on n_{salt} and is essentially independent of the salt species. Although differences in ionic radius, in principle, influence the mobility and the degree of ionization, the effect appears too small to be distinguished here. The dashed line represents the conductivity of PVC/DBA ($n_{salt} = 0$). As seen in the linear plot of σ_N *vs.* n_{salt} (Fig. 10b), σ_N converges to this base line value in the low concentration region. On this basis, we define the concentration of intrinsic carriers in the PVC/DBA gel as n_0, such that the total carrier concentration is given by $n_{sum} = n_{salt} + n_0$. Assuming σ_N is proportional to n_{sum} at low concentrations, n_0 was estimated by adjusting the σ_N *vs.* n_{sum} plot to pass through the origin. This analysis yielded $n_0 = 1.01 \times 10^{-6}$ mol g^{-1}.

While the exact nature of the charge carriers responsible for electrical conduction in the PVC/DBA gel remains unclear, assuming their mobility is comparable to that of the added salts used in this study, the concentration of intrinsic carriers is estimated to be less than one-fifth of the added salt concentration (n_{salt} = 5.345×10^{-6} mol g^{-1}) employed in the electric field response experiments. This estimation reinforces the conclusion, consistent with σ_N results (Fig. 9c and Table 1), that the electrical response is predominantly governed by the added salt than the intrinsic carriers. This result supports the assumption that the electromechanical response under the present experimental conditions is governed primarily by the introduced salts rather than by intrinsic charge carriers originally present in the PVC/DBA gel.

3.4. Nonlinear dielectric relaxation behavior

Fig. 11 shows the frequency dependence of ε' and ε'' for PVC/DBA gel with the thickness of 1.6 mm and PVC/DBA/EMIM-TFSI gel with the thickness of 1.2 mm under various applied voltages. For the PVC/DBA/EMIM-TFSI gel, the spectra obtained at 0.001, 0.01, and 0.1 V are essentially identical, indicating that the charge accumulation in the electrical double layer increases linearly with voltage. At voltages above 1 V, however, distinct nonlinear behavior is observed: at low frequencies, both ε' and ε'' increase, suggesting the formation of a nonlinear electrical double layer and/or the occurrence of leakage currents. Fig. S2 shows the corresponding results for a gel with a tenfold higher EMIM-TFSI concentration, and a similar overall trend is observed. For the PVC/DBA gel, similar nonlinear behavior is observed, extending down to 10^{-3} Hz, as shown in Fig. 11(a) and (b). These results indicate that the electrical double layer formed under actuation conditions cannot be described within a linear dielectric framework, highlighting the importance of nonlinear interfacial polarization in the deformation mechanism.

Since gel deformation under an electric field occurs only at high voltages ($\geq$100 V mm^{-1}), the current absorption method was employed to evaluate the nonlinear dielectric properties of the PVC/DBA and PVC/DBA/EMIM-TFSI gels at 170 V (see Experimental section). Fig. 12(a) and (b) respectively show the real (ε') and imaginary (ε'') components of the dielectric constant over the frequency range from 1.6×10^{-4} to 1.4×10^{-2} Hz (ω = 0.001–0.086 s^{-1}), together with the results obtained at for voltages $\leq$0.01 V (linear region).

The ε' and ε'' values of the PVC/DBA/EMIM-TFSI gel are higher than those of the PVC/DBA gel, and the values obtained at 170 V exceed those measured at 3 V (Fig. 11). These results indicate that the dielectric constant associated with electrode polarization increases nonlinearly with applied voltage. Although the electrodes used in this study (Fig. S3) did not have a fixed spacing, and deformation of the gel could have slightly reduced the gap at 170 V, the thickness would have to decrease by more than one order of magnitude to account for the observed increase in ε' and ε'' (Fig. 12). Such a large contraction was not visually observed: therefore, the nonlinear increase is attributed to enhancement in the charge density within the electrical double layer. Here, the "effective thickness"

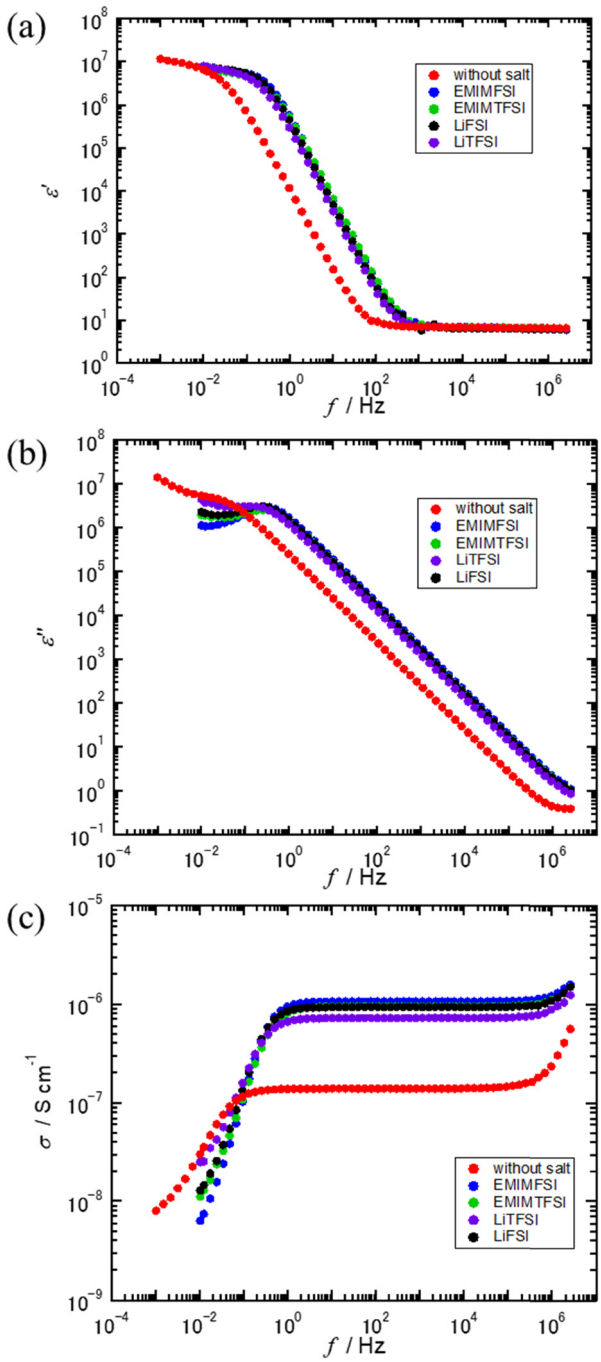

Fig. 9 Frequency dependence of (a) dielectric constant, (b) dielectric loss, and (c) conductivity for PVC/DBA gel and four types of PVC/DBA/salt gels within the linear region (0.001–0.10 V).

should be understood as the spatial range over which ions migrate to form the electrical double layer, rather than a physical contraction of the gel film. An important observation from Fig. 12 is that, at 170 V, ε' and ε'' values of the PVC/DBA/salt gels are essentially independent of the type of ion present. These results indicate that the electrical double layer formed under actuation conditions cannot be described within a linear dielectric framework, highlighting the importance of nonlinear interfacial polarization in the deformation mechanism.

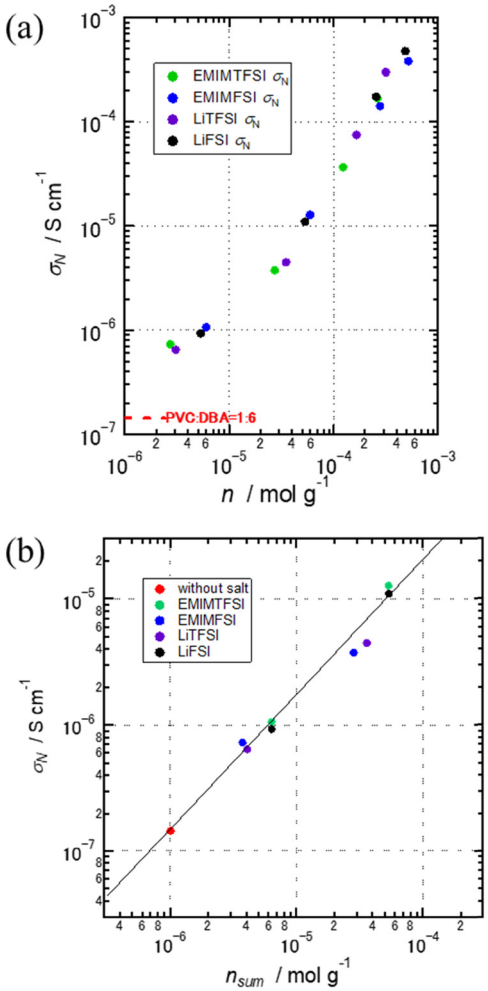

Fig. 10 (a) Salt concentration dependence of plateau conductivity. (b) Total carrier concentration dependence of plateau conductivity.

3.5. Electric field response test

The PVC : DBA ratio was varied over a wide range (9 : 1–1 : 75) in preliminary experiments. At high PVC content, the gels were mechanically stiff and exhibited limited deformation, whereas at high DBA content, they became too soft to maintain structural stability during actuation. Based on these observations, a ratio of 1 : 6 was selected as it provides a suitable balance between mechanical robustness and ionic mobility, enabling reproducible electromechanical measurements. Fig. 13(a) shows the time evolution of the bending angle $\theta(t)$, for the PVC/DBA gel and all PVC/DBA/salt gels (PVC : DBA = 1 : 6, $n = 5.35 \times 10^{-6}$ mol g^{-1}) after applying a constant electric field of 300 V mm^{-1} for 100 seconds starting at $t = 0$. The bending angle at $t = 0$, $\theta(0)$, is defined as zero. The experimental data of $\theta(t)$ were fitted using a single-relaxation mode description by eqn (10):

$$\theta_{\text{fit}}(t) = \theta_{\infty}\left(1 - e^{-t/\tau_{\theta}}\right) \quad (10)$$

where θ_{∞} is the maximum bending angle and τ_{θ} is the relaxation time of the bending process. The obtained values θ_{∞} and

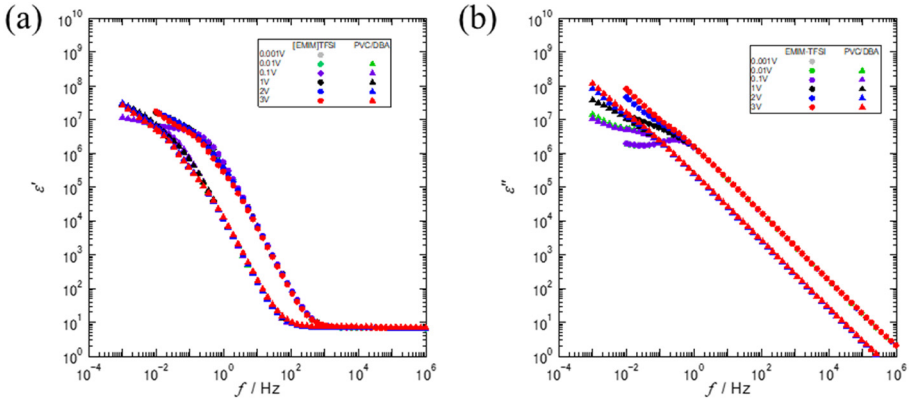

Fig. 11 Frequency dependence of (a) dielectric constant and (b) dielectric loss for PVC/DBA and PVC/DBA/EMIM-TFSI gels (PVC : DBA = 1 : 6, n_{salt} = 5.35 × 10^{-6} mol g^{-1}) under several voltage amplitudes.

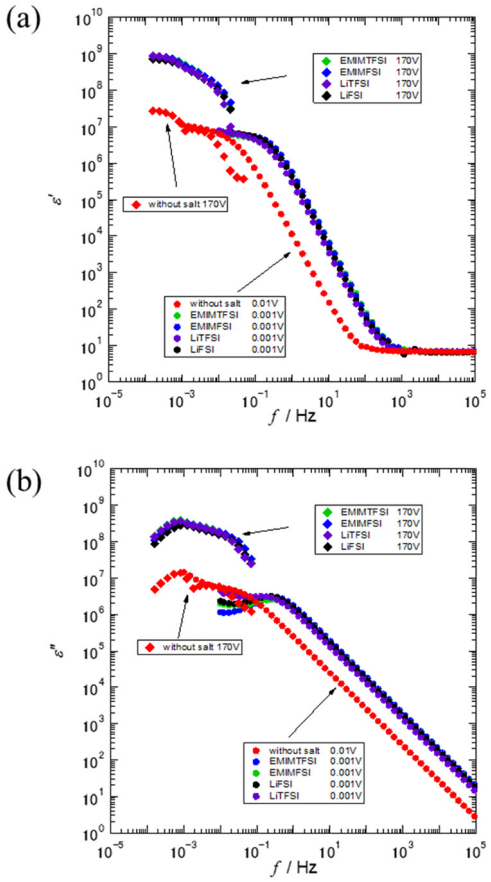

Fig. 12 (a) Dielectric constant and (b) dielectric loss for PVC/DBA and PVC/DBA/salt gels (PVC : DBA = 1 : 6, n_{salt} = 5.35 × 10^{-6} mol g^{-1}) at 0.001 V and 170 V. The thicknesses of gel samples were 1.6–1.2 mm summarized in Table S2.

τ_θ are summarized in Table S2. The fitted results are shown as dashed lines in the figure. Fig. 13(b) presents the bending angle values compensated for the slight differences in elastic moduli listed in Table 1. The compensation was performed by multiplying $\theta(t)$ by each sample's plateau modulus G_N. This result indicates that the difference in elastic moduli among the gels have only a minor influence on the observed bending behavior across the various salt systems.

Fig. 14 shows the deformation of the samples at their equilibrium state (maximum bending). All gels bent toward the anode. As previously reported for PVC/DBA gels, this bending is attributed to the accumulation of anions and/or DBA near the anode,[23] although the specific ion species have not been identified. From Fig. 13 and 14, it is evident that $\theta(t)$ values are larger for the salt-added gels. One possible explanation for this enhanced bending is that the introduction of ions increases the electric current, leading to Joule heating, softening of the gel, and consequently easier bending deformation. However, as discussed in Section S4 of the SI, the estimated temperature rise due to Joule heating is insufficient to reduce the elastic modulus of the gel, and this mechanism can therefore be excluded as the primary origin of the enhanced bending.

Regarding the anions effect, the system containing the smaller FSI^- ion exhibits greater bending than the larger $TFSI^-$ ion. In contrast, for the cation effect, the system containing the larger $EMIM^+$ ion shows greater bending than the smaller Li^+ ion system. The ion-species-dependent trend in the deformation magnitude remained unchanged even when the electric field strength was varied, as discussed in the following section. This behavior can be rationalized by considering that smaller ions produce a higher interfacial charge density, leading to stronger electrostatic attraction at the corresponding electrode interface. When the attractive force at the anode exceeds that at the cathode, the gel bends toward the anode, as schematically illustrated in Fig. 15. Because direct microscopic observation of ion distributions under operating conditions remains challenging, the proposed mechanism is inferred from indirect experimental evidence.

The observed ion-size dependence of the electromechanical response contradicts the electro-wetting model proposed by Zhen *et al.*,[30] who attributed enhanced deformation to increased ion-size asymmetry, particularly combinations of large anions and small cations, through a negative excess surface tension at the gel/anode interface under dilute ion conditions. In contrast, our systematic experiments using four representative salts show the opposite trend: gels containing smaller anions (FSI^-) and

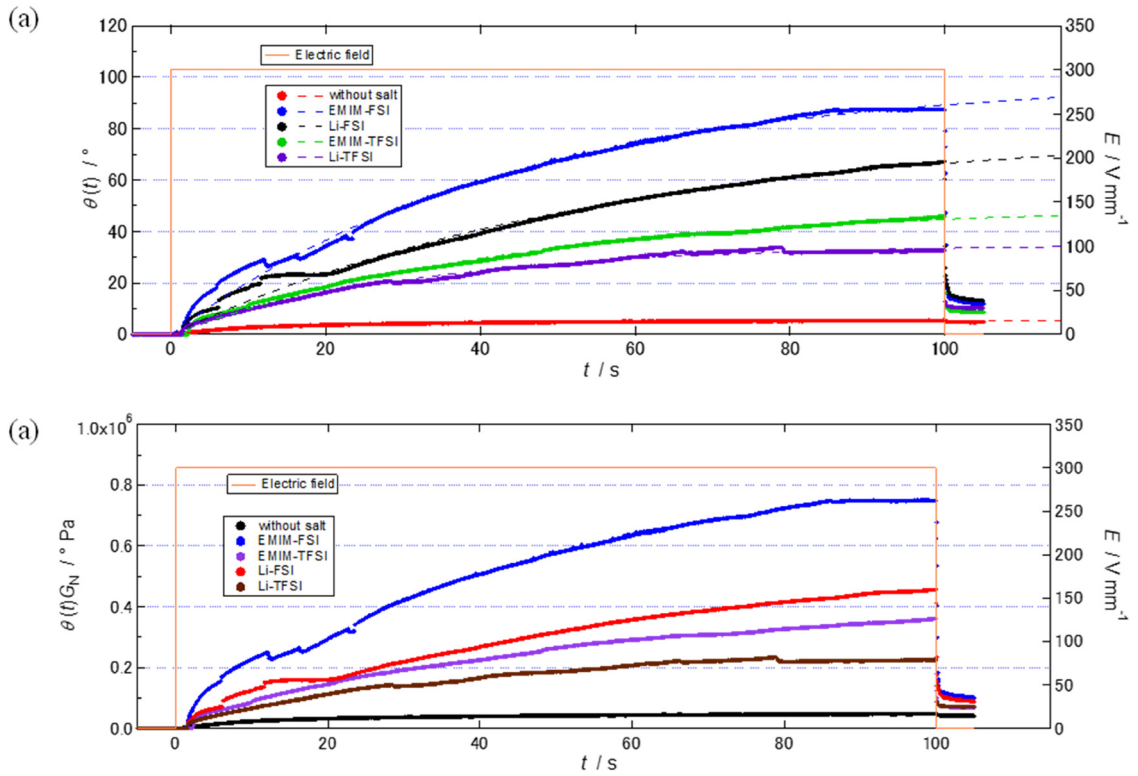

Fig. 13 Time evolution of (a) $\theta(t)$, and (b) $\theta(t) \times G_N$ for PVC/DBA gel and all PVC/DBA/salt gels (PVC : DBA = 1 : 6, $n_{salt} = 5.35 \times 10^{-6}$ mol g^{-1}) after applying a constant electric field of 300 V mm^{-1} for 100 seconds at time $t = 0$.

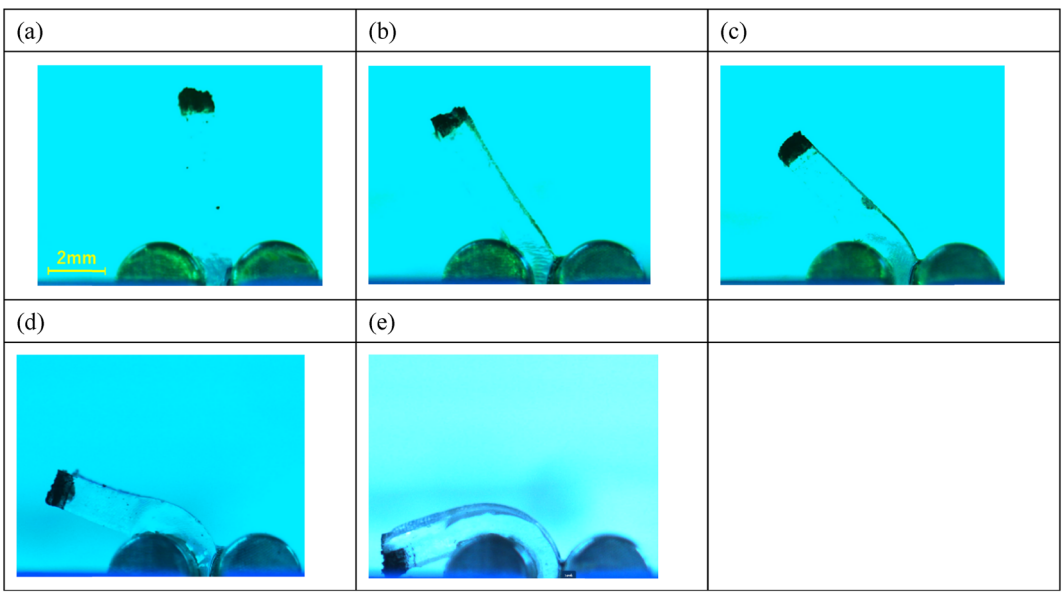

Fig. 14 Maximum bending observed when an electric field of 300 V mm^{-1} is applied to (a) PVC/DBA gel, (b) PVC/DBA/Li-TFSI gel, (c) PVC/DBA/EMIM-TFSI gel, (d) PVC/DBA/Li-FSI gel, and (e) PVC/DBA/EMIM-FSI gel.

larger cations ($EMIM^+$) exhibit the largest bending deformation. This discrepancy likely arises from the different physical regimes considered. Whereas Zheng *et al.* focused on interfacial effects under dilute ion assumptions, the salt concentrations employed in this study significantly enhance bulk conductivity, suggesting that ion accumulation at the electrodes approaches saturation. Further studies covering a broader range of ion sizes will be necessary to assess the generality of this behavior.

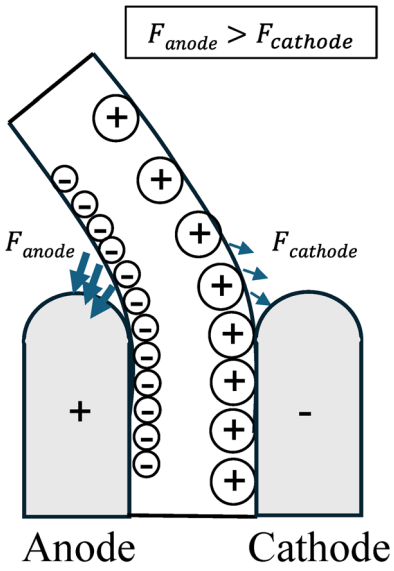

Fig. 15 Schematic illustration of asymmetric electric double layers formed under a high electric field. Smaller ions generate higher interfacial charge density, resulting in a stronger electrostatic attraction at the electrode interface. The blue arrows indicate the electrostatic attractive forces acting between the accumulated charges in the gel and the electrodes. Because the attractive force at the anode side (F_{anode}) exceeds that at the cathode side ($F_{cathode}$), the gel bends toward the anode.

Dielectric measurements reveal that, under high electric fields, the low-frequency dielectric constant associated with electrode polarization becomes nearly independent of ion species. At first glance, this appears inconsistent with the pronounced ion-dependent bending deformation. However, the dielectric constant reflects the overall extent of charge polarization and does not uniquely determine the spatial distributions of cations and anions. As schematically illustrated in Fig. 15, ion-size-dependent asymmetry in the electric double layers can arise, even when the dielectric constants are comparable. Such asymmetric charge distributions generate unequal Coulombic forces at the anode and cathode interfaces, resulting in net bending toward the anode. These findings indicate that, under experimentally relevant high-field and finite-ion-concentration conditions, PVC gel actuation cannot be explained solely by an electro-wetting mechanism based on total interfacial charge. Instead, asymmetric Coulombic forces originating from ion-size-dependent spatial distributions dominate the electromechanical response. In addition, possible accumulation of the plasticizer DBP near the cathode side cannot be completely ruled out and may further enhance the asymmetry of the electrostatic interaction.

This interpretation is also consistent with the thickness dependence of the bending behavior shown in Fig. S8 in the SI. Under the same electric field strength, thicker gels exhibited larger bending deformation despite their larger bending rigidity and longer ion migration distance. In addition, the thickest gel/highest-voltage condition showed a non-monotonic transient response, suggesting the presence of additional nonlinear interfacial effects under high-voltage conditions. These observations further support the view that PVC gel actuation is governed not only by bulk ion transport, but also by interfacial charge distributions and local electric-field effects.

To obtain preliminary insight into the cyclic durability of the actuation behavior, repeated bending tests were additionally performed for the salt-free PVC/DBA gel and the PVC/DBA/EMIM-FSI gel, which exhibited the largest bending deformation. The results are presented in Fig. S7 in the SI. Although the addition of EMIM-FSI significantly enhances the bending deformation, the deformation amplitude decreased markedly during repeated cycling compared with the salt-free system. These results suggest that ion addition improves the actuation magnitude but may simultaneously reduce the cyclic stability of the electromechanical response. Because cyclic tests were not systematically performed for all salt systems, these observations should be regarded as preliminary results.

Fig. 13 also shows the deformation recovery behavior after the electric field is turned off at t = 100 s. As evident from the figure, the recovery occurs much faster than the deformation process. The deformation is governed by ion migration and the gradual development of an asymmetric charge distribution near the electrodes, which is limited by ionic diffusion and the formation of electric double layers. In contrast, once the electric field is removed, the electrostatic forces vanish instantaneously, and the gel rapidly returns to a nearly original shape, driven by the release of stored elastic energy. As a result, the recovery process is significantly faster than the deformation process. This rapid recovery behavior also suggests that large-scale redistribution of the plasticizer DBA is unlikely to be the primary origin of the deformation. If substantial DBA migration or macroscopic concentration redistribution occurred during deformation, a much slower relaxation process associated with molecular diffusion would be expected after removal of the electric field. Therefore, although possible local redistribution of DBA near the electrode interface cannot be completely ruled out, the present results support the view that asymmetric electrostatic forces associated with ion-size-dependent charge distributions play the dominant role in the bending deformation.

3.6. Electric field strength dependence

Fig. 16(a) and (b) show how θ_∞ and τ_θ change with the electric field strength E, respectively, for each ion species. It was found that θ_∞ increases with the first to second power of E. Moreover, the order of bending shown in Fig. 14 is maintained at all electric field strength. In contrast, τ_θ tends to decrease with increasing E in the salt-free system, whereas it increases in the salt-containing systems. If the deformation of the PVC gel occurs in association with ion migration and the formation of an electric double layer, as schematically illustrated in Fig. 15, the process is likely governed by ion transport. In this case, an increase in the electric field strength enhances the ion drift velocity, leading to a faster electromechanical response. Such behavior is indeed observed in the salt-free PVC gel, where the ion concentration is relatively low.

In contrast, at higher ion concentrations, it may take a longer time for a thick electrical double layer to be established

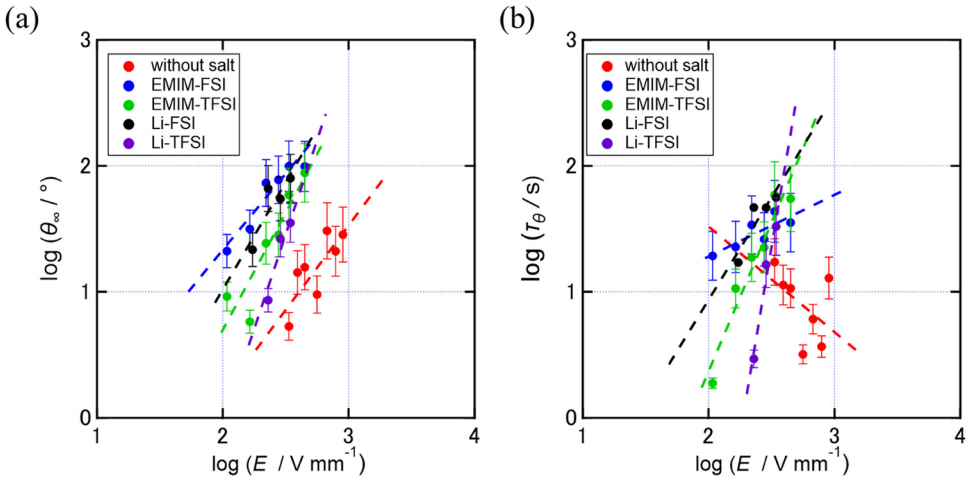

Fig. 16 Dependence of maximum bending angle θ_∞ (a), and relaxation time τ_θ (b) on the electric field strength for PVC/DBA/salt gels (PVC : DBA = 1 : 6, n_{salt} = 5.35 × 10^{-6} mol g^{-1}).

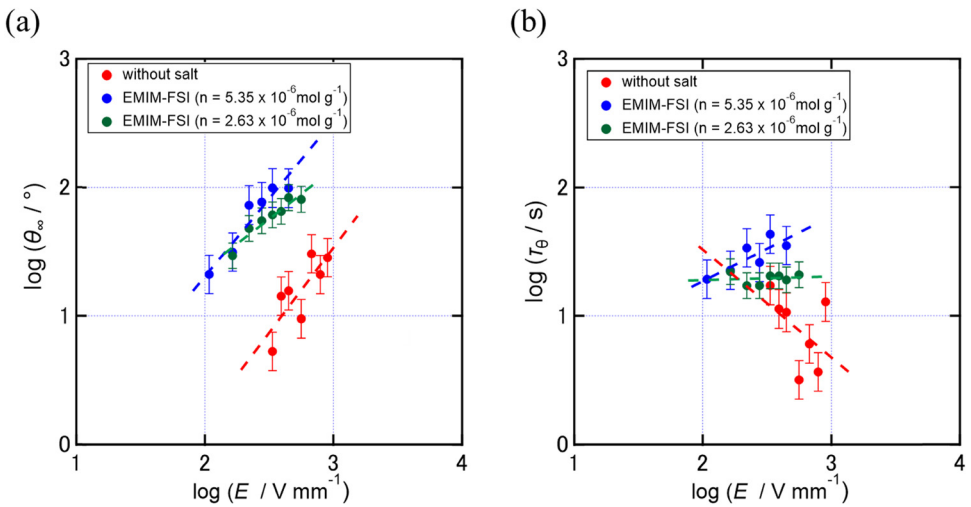

Fig. 17 Dependence of maximum bending angle θ_∞ (a) and relaxation time τ_θ (b) on the electric field strength for PVC/DBA/EMIM-FSI gels with varying salt concentration (n_{salt} = 0,2.68 × 10^{-6}, and 5.35 × 10^{-6} mol g^{-1}).

under high electric fields. As shown in Fig. 12, the dielectric constant of the salt-containing gels increases markedly in the low-frequency region under high electric fields, and it reaches a plateau only at around 10^{-2} Hz, which is an extremely low frequency and corresponds to the time scale of the gel deformation shown in Fig. 16(b). This behavior suggests that the formation of the electrical double layer requires a long time. Fig. 17(a) and (b), respectively, presents the dependence of θ_∞ and τ_θ on the electric field strength for the EMIM-FSI–doped PVC gels, including the sample with half the ion concentration. A closer look at τ reveals that the slope of its dependence on the electric field strength changes from positive to negative as the ion concentration decreases, which is consistent with the above hypothesis.

As shown in Fig. S2, the nonlinear dielectric relaxation behavior of the EMIM-TFSI system at a higher salt concentration shows that, even under a moderate applied voltage up to 3 V, both ε' and ε'' increase with increasing voltage in the low-frequency region corresponding to electrode polarization. In this case, the typical low-frequency plateau of ε' is no longer observed within the frequency range. These results suggest that increasing in salt concentration prolongs the timescale required to establish a steady electrical double layer, which is consistent with the behavior observed in Fig. 17(b).

4. Conclusion

In this study, we systematically investigated the electromechanical behavior of PVC/DBA gels containing salts with controlled ion sizes. The addition of ionic liquids effectively enhanced the bending response of the gels, achieving deformation more than five times greater than that of the salt-free system, even under low electric fields.

Dielectric analysis revealed that the low-frequency dielectric constant under high voltage was almost independent of the salt species, indicating that the total charge accumulation at the electrodes reaches a similar level among the systems. Nevertheless, the degree of deformation strongly depended on ion size: gels containing smaller anions (FSI^-) and larger cations ($EMIM^+$) exhibited the largest bending. This result suggests that the asymmetric spatial distribution of cations and anions in the electrical double layer determines the magnitude of the electrostatic force acting on the gel, leading to ion-species-dependent deformation. The possible accumulation of the solvent (DBA) near the cathode side may further contribute to this asymmetry.

Furthermore, analysis of the field-strength dependence of the relaxation time revealed opposite trends between salt-free and salt-containing systems: in the former, the response becomes faster with increasing electric field, while in the latter, the relaxation slows down. This contrast can be rationalized by a transition from a drift-limited regime at low ion concentrations to a diffusion-limited regime at high ion concentrations, where the establishment of a thick and steady electrical double layer requires a longer timescale.

Overall, this study demonstrates that controlling ion size and concentration provides an effective strategy for tuning the electromechanical performance of PVC gels. The electromechanical response is governed by asymmetric Coulombic forces arising from ion-specific spatial distributions within the electrical double layer, rather than by total interfacial charge. The insights gained here clarify the interplay between ion migration, double-layer formation, and mechanical deformation, and offer fundamental design guidelines for next-generation low-voltage soft actuators.

Conflicts of interest

There are no conflicts to declare.

Data availability

The data supporting the findings of this study are available within the article and its supplementary information (SI). Supplementary information is available. See DOI: https://doi.org/10.1039/d6sm00031b.

Additional raw data are available from the corresponding author upon reasonable request.

References

1 Y. Osada, H. Okuzaki and H. Hori, *Nature*, 1992, **355**, 242–244.
2 M. A. C. Stuart, W. T. S. Huck, J. Genzer, M. Müller, C. Ober, M. Stamm, G. B. Sukhorukov, I. Szleifer, V. V. Tsukruk, M. Urban, F. Winnik, S. Zauscher, I. Luzinov and S. Minko, *Nat. Mater.*, 2010, **9**, 101–113.
3 L. Hines, K. Petersen, G. Z. Lum and M. Sitti, *Adv. Mater.*, 2017, **29**, 1603483.
4 J. W. Bae, E.-J. Shin, J. Jeong, D.-S. Choi, J. E. Lee, B. U. Nam, L. Lin and S.-Y. Kim, *Sci. Rep.*, 2017, **7**, 2068.
5 Q. Shi, H. Liu, D. Tang, Y. Li, X. Li and F. Xu, *NPG Asia Mater.*, 2019, **11**, 64.
6 H. Sato and T. Hirai, *Electromechanical and electro-optical functions of plasticized PVC with colossal dielectric constant*, SPIE, 2013.
7 Y. H. Liu, Z. Q. Shi, X. Y. Yue, J. Zhao, X. Y. Zhao, X. Y. He, Z. W. Guo, Z. M. Zhang, Y. J. Xie, W. Yu, X. Z. Yan and Z. Liang, *J. Am. Chem. Soc.*, 2026, **148**, 1570–1580.
8 G. Park, B. Kim, J. Lee and J. Kim, *Int. J. Precis. Eng. Manuf. - Green Technol.*, 2025, DOI: 10.1007/s40684-025-00809-x.
9 D. Cao, D. He, Y. Zhao, D. Jin, J. Zhang and W. Wang, *SmartBot*, 2026, DOI: 10.1002/smb2.70026.
10 M. F. Siddique, F. K. Omar and A. H. Al-Marzouqi, *Gels*, 2026, **12**, 138.
11 Y. Li, Z. Q. Zhang, H. Z. Zhu, J. X. Sun, M. F. Guo, X. Zeng, Y. B. Li and M. Hashimoto, *Sens. Actuators, B*, 2026, **447**, 138894.
12 Z. Jin, X. Wei, X. He, Z. Wang, Z. Zhao, H. He, Y. Yang and N. Chen, *Materials*, 2024, **17**, 4204.
13 D. Han, C. Farino, C. Yang, T. Scott, D. Browe, W. Choi, J. W. Freeman and H. Lee, *ACS Appl. Mater. Interfaces*, 2018, **10**, 17512–17518.
14 T. Shiga, *Adv. Polym. Sci.*, 1997, **134**, 131–163.
15 S. Nemat-Nasser and Y. X. Wu, *J. Appl. Phys.*, 2003, **93**, 5255–5267.
16 I. S. Park, S. M. Kim, D. Pugal, L. M. Huang, S. W. Tam-Chang and K. J. Kim, *Appl. Phys. Lett.*, 2010, **96**, 043301.
17 M. Annabestani, N. Naghavi and M. Maymandi-Nejad, *Sci. Rep.*, 2021, **11**, 6435.
18 J. D. Madden, in *Electroactive Polymers for Robotic Applications: Artificial Muscles and Sensors*, ed. K. J. Kim and S. Tadokoro, Springer London, London, 2007, pp. 121–152, DOI: 10.1007/978-1-84628-372-7_5.
19 E. Smela, *Adv. Mater.*, 2003, **15**, 481–494.
20 D. X. Wang, C. Lu, J. J. Zhao, S. Han, M. H. Wu and W. Chen, *RSC Adv.*, 2017, **7**, 31264–31271.
21 T. Fukushima, A. Kosaka, Y. Ishimura, T. Yamamoto, T. Takigawa, N. Ishii and T. Aida, *Science*, 2003, **300**, 2072–2074.
22 N. Terasawa and K. Asaka, *Langmuir*, 2016, **32**, 7210–7218.
23 H. Xia, M. Takasaki and T. Hirai, *Sens. Actuators, A*, 2010, **157**, 307–312.
24 M. Ali and T. Hirai, *Soft Matter*, 2012, **8**, 3694–3699.
25 Y. Li and M. Hashimoto, *Sens. Actuators, A*, 2015, **233**, 246–258.
26 K. Asaka and M. Hashimoto, *Sens. Actuators, B*, 2018, **273**, 1246–1256.
27 H. Xia and T. Hirai, *J. Phys. Chem. B*, 2010, **114**, 10756–10762.
28 M. Ali, T. Ueki, D. Tsurumi and T. Hirai, *Langmuir*, 2011, **27**, 7902–7908.

29 M. Ali and T. Hirai, *Soft Matter*, 2012, **8**, 3694.
30 B. Zheng, X. Man, D. Andelman and M. Doi, *ACS Macro Lett.*, 2021, **10**, 498–502.
31 C. S. Bian, Z. C. Zhu, W. F. Bai, H. L. Chen and Y. Li, *Smart Mater. Struct.*, 2020, **29**, 035014.
32 Z. Frank and K. J. Kim, *Sci. Rep.*, 2022, **12**, 10316.
33 T. Hwang, Z. Frank, J. Neubauer and K. J. Kim, *Sci Rep-Uk*, 2019, **9**, 9658.
34 S. H. Chen, M. W. M. Tan, X. F. Gong and P. S. Lee, *Adv. Intell. Syst. Ger.*, 2022, **4**, 2100075.
35 J. E. Martin, D. Adolf and J. P. Wilcoxon, *Phys. Rev. A: At., Mol., Opt. Phys.*, 1989, **39**, 1325–1332.
36 M. Muthukumar, *Macromolecules*, 1989, **22**, 4656–4658.
37 M. Rubinstein, R. H. Colby and J. R. Gillmor, *Springer Series Chem.*, 1989, **51**, 66–74.
38 J. R. Macdonald, *J. Chem. Phys.*, 1973, **58**, 4982–5001.
39 R. J. Klein, S. H. Zhang, S. Dou, B. H. Jones, R. H. Colby and J. Runt, *J. Chem. Phys.*, 2006, **124**, 144903.
40 Y. Matsumiya, N. P. Balsara, J. B. Kerr, T. Inoue and H. Watanabe, *Macromolecules*, 2004, **37**, 544–553.